ELSEVIER

Chemical Geology 212 (2004) 209–228

CHEMICAL GEOLOGY
INCLUDING
ISOTOPE GEOSCIENCE

www.elsevier.com/locate/chemgeo

Adsorption of ferrous ions onto *Bacillus subtilis* cells

Xavier Châtellier[a,*], Danielle Fortin[b]

[a]*CNRS, UMR 6118, Géosciences Rennes, Université de Rennes 1, Campus de Beaulieu, F-35042 Rennes Cedex, France*
[b]*Department of Earth Sciences, University of Ottawa, Ottawa, ON, Canada, K1N 6N5*

Received 28 January 2004; accepted 16 August 2004

Abstract

Bacteria are known to have reactive surfaces that can affect the cycling of dissolved elements through sorption reactions. The properties of adsorption of various metallic ions (Cd^{2+}, Pb^{2+}, etc.) onto various types of Gram-positive or -negative bacterial surfaces have been measured in several previous studies, but the behavior of ferrous ions has been somewhat left out, possibly because ferrous ions are easily oxidized under standard laboratory conditions. In this paper, the adsorption of ferrous ions onto *Bacillus subtilis* (a Gram-positive bacterium) was measured under anoxic conditions as a function of pH for various Fe(II)/bacteria ratios. Our results first indicate that Fe(II) adsorption increased with pH and that the adsorption was reversible. An equilibration time of one hour was found sufficient to reach equilibrium between the bacterial surfaces and the solution. Acid–base titrations of the bacterial suspensions were also performed. The titration data could be fitted using a simple three-site model. Neglecting the electrostatic component, the three sites had pK values of 4.45 (pK_1), 6.74 (pK_2), and 9.08 (pK_3) with corresponding concentrations of 5.6, 5.3, and 6.1 ($\times 10^{-4}$ mol/dry g of bacteria), respectively. The high density of sites available for proton adsorption suggests that protons can easily diffuse within the cell walls. The adsorption data for Fe(II) was fitted with a single-site model. A Langmuir adsorption isotherm suggested that the site concentration available for the adsorption of the ferrous ions was equal to 3.5×10^{-4} mol/g which as far less than for protons. The modeling analysis of the adsorption isotherms also indicated that the adsorption took place onto the type 2 sites (pK_2=6.74), or type 3 sites (pK_3=9.08) and that the adsorption constant of the Fe(II) ions onto the protonated sites was equal to $-\log(T')=-1.22\pm0.10$. A two-site model did not improve the quality of the fit, but indicated that the type 1 sites (pK_1=4.45) could contribute only to a limited extent to the adsorption process.

Keywords: Ferrous ions; Adsorption; Adsorption isotherms; Desorption; FITEQL 2.0; Constant capacitance model; *Bacillus subtilis*; Bacteria

1. Introduction

Bacteria are ubiquitous in low-temperature surface environments (Madigan et al., 2003). Because of their small size, they have a high surface area per unit

* Corresponding author. Tel.: +33 223 5269; fax: +33 223 23 6090.
E-mail address: xavier.chatellier@univ-rennes1.fr (X. Châtellier).

0009-2541/$ - see front matter © 2004 Elsevier B.V. All rights reserved.
doi:10.1016/j.chemgeo.2004.08.013

weight. Considering that they tend to colonize mineral surfaces as well as travel in the aqueous phases, they can represent a significant fraction of the reactive surface area available for the adsorption of dissolved molecules or the adhesion of nanominerals, provided that their concentration is large enough. Bacteria are, for instance, believed to play a significant role in the cycling of multivalent inorganic cations, such as lead or cadmium ions, which can sorb onto their surfaces (Boyanov et al., 2003; Daughney and Fein, 1998; Daughney et al., 2001; Fein et al., 1997, 2001; Kelly et al., 2001, 2002; Kulczycki et al., 2002; Martinez and Ferris, 2001; Ngwenya et al., 2003; Yee and Fein, 2001). They are also known to affect the dissolution of mineral phases (Lovley, 2000; Roden and Urrutia, 2002; Shelobolina et al., 2003; Southam, 2000), or the precipitation of secondary solid phases, such as amorphous silica, and of iron or manganese oxides. In precipitation reactions, bacteria are thought to play a nonmetabolic role, by offering their reactive surfaces for nucleation or adhesion and growth of crystal nuclei, and, in some instances, a more active role, by taking part metabolically in the chemical reactions leading to the precipitation of the mineral phases (Châtellier et al., 2001, 2004; Emerson, 2000; Ferris et al., 1986; Fortin and Ferris, 1998; Fortin et al., 1997, 1998; Francis and Tebo, 2002; Kennedy et al., 2003; Schultze-Lam et al., 1996; Yee et al., 2003). The exact mechanisms through which bacteria can contribute to the dissolution of iron minerals or to their precipitation are still under investigation. For instance, it is still not clear when iron-oxide nanocrystals nucleate directly onto the bacterial cell walls and when they nucleate in the bulk (Châtellier et al., 2001, 2004). It is also believed that adsorption of ferrous ions onto bacterial cells can inhibit their ability to reduce ferric iron minerals (Liu et al., 2001; Roden and Urrutia, 2002; Urrutia and Roden, 1998). To investigate these questions, it is important to understand how ferrous and ferric ions adsorb onto and desorb from bacterial surfaces. The adsorption of ferric ions onto *Bacillus subtilis* has recently been investigated by Daughney et al. (2001) at low pH, i.e., in the pH range where the ferric ions are still relatively soluble. The adsorption of ferrous ions onto bacterial cells has been quantitatively studied only in the form of Langmuir isotherms at neutral pH (Liu et al., 2001; Roden and Urrutia, 2002; Urrutia and Roden, 1998). As a result, we investigated experimentally the thermodynamics and kinetics of adsorption of ferrous ions onto *B. subtilis* cells under anoxic conditions at various pH and various bacteria/Fe(II) ratios. An acid–base titration was also performed to relate the reactivity of the bacterial surfaces towards protons and towards ferrous ions, and the titration data and the adsorption isotherms were modeled using a surface complexation model (SCM).

2. Materials and methods

2.1. Anaerobic solutions

Anaerobic water was prepared by boiling ultrapure water for 10 minutes, transferring it into an anaerobic chamber with a 5% H_2/95% N_2 atmosphere, and bubbling it with the same gas mixture while stirring vigorously for another 5 h. All anaerobic solutions, such as anaerobic electrolyte solutions (NaCl), were prepared using anaerobic water and were stored under anaerobic conditions. A palladium catalyst was replaced daily in the chamber in order to continuously remove the traces of oxygen, which might have penetrated it. The Fe(II) stock solution was prepared by dissolving 1.00×10^{-3} mol of $FeCl_2$ in 1 ml of 1 M HCl, to which 999 ml of an anaerobic 10^{-3} M NaCl solution were added. The pH of the stock solution was kept low (pH 3) in order to prevent the oxidation of the ferrous ions in case of oxygen contamination. As the equilibrium concentration of oxygen in aqueous solutions in contact with the atmosphere is on the order of 2.65×10^{-4} M (Langmuir, 1997), and because the 1 M HCl solution used to dissolve the iron(II) salt was diluted 1000 times, the initial concentration of oxygen in the $FeCl_2$ stock solution was likely on the order of 2.65×10^{-7} M. Given that 1 mol of oxygen can oxidize 4 mol of ferrous ions (Cornell and Schwertmann, 2003), we estimated that the maximal production of iron(III) in the stock solution was on the order of 10^{-6} M, which we deemed to be negligible. Anaerobic solutions of NaOH (10^{-2} and 10^{-3} M) and HCl (10^{-2} and 10^{-3} M) were prepared by diluting 1.0 N standard NaOH and HCl solutions in anaerobic 10^{-3} M NaCl. The acid solutions were then stirred overnight in the anaerobic chamber, in order to remove the trace

amounts of oxygen coming from the 1.0 N HCl standard solution.

2.2. Bacterial suspensions

B. subtilis cells (ATCC 168) were grown in 2 l of Tryptic Soy Broth (Difco, 30g/l) containing yeast extract (Difco, 5 g/l), according to the protocol described by Daughney and Fein (1998), and were harvested after 7.5 h, while in exponential phase. The culture was removed from the growth medium by centrifugation at 6000 rpm for 15 min (equivalent to about 12 700×g), washed three times in 250 ml of 10^{-3} M NaCl, then three times in 250 ml of anaerobic 10^{-3} M NaCl, and finally once in 100 ml of anaerobic 10^{-3} M NaCl. Emptying of the supernatants was carried out under anaerobic atmosphere from the fourth centrifugation on. The optical density of the bacterial stock suspension was measured at 600 nm using a 1% dilution of the suspension in 10^{-3} M NaCl. The dry weight of the stock bacterial suspension was determined by drying two samples (15 ml each) for 2 weeks at 60 °C.

2.3. Acid–base batch titration

The samples were prepared under anaerobic conditions by mixing in borosilicate glass vials the bacterial suspension (dry weight concentration of 570 mg/l), known quantities of anaerobic NaOH or HCl solutions, and 10^{-3} M NaCl, in order to bring the total volume to 20 ml. Samples were gently agitated on a rotary shaker for 60 minutes based on our kinetic experiments (see Sections 2.4.3 and 3.2), after which the pH was measured in the samples. Anaerobic conditions were maintained throughout the experiment, and different vials were used for the different amounts of base or acid added.

2.4. Adsorption/desorption experiments

2.4.1. Adsorption experiments

The samples were prepared under anaerobic conditions by mixing in borosilicate glass vials 2 ml of 10^{-3} M $FeCl_2$, the bacterial suspension (dry weight concentration of 50 mg/l, 500 mg/l, or 5g/l, as estimated from the measurement of the absorbance at 600 nm), known quantities of anaerobic NaOH or HCl solutions, and 10^{-3} M NaCl, in order to bring the total volume to 20 ml. The initial concentration of dissolved Fe(II) was 10^{-4} M. Samples were gently agitated on a rotary shaker for 60 min, except during our kinetic experiments where the equilibration time was varied (see Section 3.2). At the end of the mixing period, 12 ml of the sample was filtrated with a 0.2-μm surfactant-free cellulose acetate filter, while the pH was measured in the remainder of the suspension. The pH was measured using a Ross Sure-Flow Electrode (Orion) and recorded after 120 s of equilibration. The filtrate was immediately analyzed for Fe(II) and total Fe using the ferrozine method according to the method of Viollier et al. (2000). For the measurement of the Fe(II) concentration, 0.5 ml of an anaerobic reactive solution (10^{-2} M of ferrozine and 10^{-1} M of ammonium acetate) was added to 5 ml of the filtrate and the absorbance of the solution was recorded at 562 nm. The absorbance is proportional to the concentration of Fe(II). The slope of the curve was obtained by calibrating the method with $FeCl_2$ solutions of known concentrations. For the measurement of the total Fe concentration, 0.5 ml of an anaerobic reactive solution (10^{-2} M of ferrozine and 10^{-1} M of ammonium acetate) and 1 ml of a reducing solution (1.4 M hydroxylamine hydrochloride and 2.0 N of HCl) were added to 5 ml of the filtrate. The solution was allowed to react for 18 h to complete the reduction of Fe(III), 0.5 ml of a buffer solution (10 M of ammonium acetate adjusted to pH 9.5 with NaOH) was added to the mixture, and its optical density was measured at 562 nm. The percentage of adsorbed Fe(II) was estimated as:

$$\%\ \text{of absorbed Fe(II)} = \frac{\text{Absorbance of the blank sample} - \text{Absorbance of the biological sample}}{\text{Absorbance of the blank sample}} \quad (1)$$

where the blank sample corresponded to a sample adjusted to pH 4±1 with [Fe(II)]=10^{-4} M but without any bacteria. The amount of oxidized iron was estimated by comparing the absorbances obtained for the reduced and the unreduced samples, and it was found that the dissolved concentration of Fe(III) was always smaller than 10^{-5} M. The oxidation was thus a rather limited process, with little effect on the shape of the adsorption isotherm. Indeed, the results obtained

for the adsorption isotherm for total iron nearly overlapped the results obtained for the adsorption of Fe(II) for the same experiment (data not shown).

The Langmuir isotherm was also measured at roughly neutral pH for a bacterial concentration of 500 mg/l. Increasing amounts of ferrous ions were added to the suspension, together with NaOH, in order to reach a final pH around 7. The rest of the protocol was unchanged, except that the filtrates corresponding to the highest introduced concentrations of ferrous ions were diluted in anaerobic 10^{-3} M NaCl for Fe(II) and Fe(III) determinations using the ferrozine method. The dilution was likely a source of imprecision, but it ensured that the measured samples were always within the range of linearity of the ferrozine method. In the realization of a Langmuir isotherm, it was difficult to predict in advance the exact amount of base to be added to reach a final pH of 7.0. In order to limit the variability of our results, we discarded the data that were not in the pH range from 6.5 to 7.5.

2.4.2. Desorption experiments

For the measurement of the desorption isotherm, NaOH was first added to all samples to bring the pH to about 8.1 (8.8 for the blank sample) and the samples were stirred for 60 minutes (see Sections 2.4.3 and 3.2). Increasing amounts of HCl were then added to decrease the pH and the volume was adjusted to 20 ml. After a second period of 60 min, the pH was measured and the samples were filtrated for the analysis of Fe(II) and total Fe. It was found that up to about 5% of the Fe(II) was still adsorbed on the walls of the glass container at the end of the experiment. Eq. (1) was used to take into account this artifact, but, with this procedure, the percentage of adsorbed Fe(II) might have been underestimated by up to 5% in the desorption isotherm.

2.5. Modeling methods

The titration and adsorption data were modeled using a surface complexation model (SCM; Daughney and Fein, 1998; Fein et al., 1997, 2001; Kulczycki et al., 2002; Martinez and Ferris, 2001; Yee and Fein, 2001). We considered that bacteria interact with protons via monoprotic acid–base reactions and that the ferrous ions adsorb onto single sites rather than onto two ligands. In this paper, we neglected the charge excess for each ion in the double layer close to the bacterial surfaces. The bacterial surfaces were considered to be covered with m types of reactive sites, each site i corresponding to a certain chemical group R_i and being characterized by a concentration c_i (in moles of sites per dry g of bacteria), and constants of adsorption K_i and T_i for the protons and for the cations respectively, such as:

$$R_i + \mathrm{H}^+ \rightarrow R_i - \mathrm{H}^+ \quad \text{and} \quad R_i + \mathrm{Fe}^{2+} \rightarrow R_i - \mathrm{Fe}^{2+} \tag{2}$$

$$K_i = \frac{[R_i][\mathrm{H}^+]}{[R_i - \mathrm{H}^+]} 10^{-\psi_0} \quad \text{and} \quad T_i = \frac{[R_i][\mathrm{Fe}^{2+}]}{[R_i - \mathrm{Fe}^{2+}]} 10^{-2\psi_0} \tag{3}$$

where $\psi_0 = eV_0/(kT\ln(10))$, V_0 is the electrostatic potential at the bacterial surfaces, and the associated Boltzmann factors account for the electrostatic attraction or repulsion of the charged bacteria towards dissolved ions. In Eq. (2), R_i may be either neutral or charged. Instead of T_i, it is often useful to use the constant of adsorption of the ferrous ions onto the protonated sites T_i, which corresponds to the reaction:

$$R_i - \mathrm{H}^+ + \mathrm{Fe}^{2+} \rightarrow R_i - \mathrm{Fe}^{2+} + \mathrm{H}^+ \tag{4}$$

and is thus defined by:

$$T_i' = \frac{[R_i - \mathrm{H}^+][\mathrm{Fe}^{2+}]}{[R_i - \mathrm{Fe}^{2+}][\mathrm{H}^+]} 10^{-\psi_0} = \frac{T_i}{K_i} \tag{5}$$

For convenience, we will denote in the following $\bar{K}_i = K_i \cdot 10^{\psi 0}$, $\bar{T}_i = T_i \cdot 10^{2\psi 0}$, and $\bar{T}_i' = T_i' \cdot 10^{\psi 0} = \bar{T}_i / \bar{K}_i$.

2.5.1. Modeling of the titration data

The charge Q_{exp} of the bacterial surfaces can be estimated from the experimental titration data by writing the law of electroneutrality, which reads:

$$Q_{\mathrm{exp}} = [\mathrm{OH}^-] - [\mathrm{H}^+] + c_{\mathrm{a}} - c_{\mathrm{b}} + \alpha, \tag{6}$$

where c_{a} and c_{b} are the concentrations of introduced acid and base, $[\mathrm{H}^+]$ and $[\mathrm{OH}^-]$ are the bulk concentrations of H^+ and OH^-, and α is the concentration of negative charges due to the presence of anions others than OH^- minus the concentration of positive charges due to the presence of cations others than H^+, that there would be in the suspension if no acid nor base was introduced. The term α is

usually neglected in Eq. (6) (Stumm and Morgan, 1996), possibly because α is a constant in an acid–base titration, contrary to the other variables of Eq. (6). Alternatively, for a bacterial suspension of concentration c_{bact}, the charge Q_{calc} of the bacterial surfaces can be calculated as:

$$Q_{calc} = Q_0 - c_{bact} \sum_{i=1}^{m} c_i \frac{10^{-p\bar{K}_i}}{10^{-p\bar{K}_i} + 10^{-pH}} \quad (7)$$

where the sum is made over the different sites i, and Q_0 is the charge of the bacterial surfaces at low pH, when all the sites are protonated. Various models can be used to estimate the term ψ_0 (Martinez et al., 2002; Westall and Hohl, 1980). In this paper, we considered the simple model that consists in considering that ψ_0 is a constant over the pH range studied. In this case, the $p\bar{K}_i$ values are constant. The concentrations and the values of the reactive sites were estimated by comparing Eqs. (6) and (7), and finding the values of c_i, $p\bar{K}_i$, and Q_0, which led to the best agreement between Q_{exp} and Q_{calc}. It should be noted that the modeling of a titration curve does not allow to determine the value of the parameter α or the charge of the bacterial cells. Only $Q_0-\alpha$ and the variations of the charge can be estimated. The quality of a model with n data points was measured by computing the quantity:

$$\Delta = \sqrt{\sum_{j=1}^{n} \frac{\left(Q^j_{calc} - Q^j_{exp}\right)^2}{n}} \quad (8)$$

If the difference between the value of the charge as predicted by the model and as found experimentally is equal for every data point to d, then $\Delta=d$. Hence, Δ is referred to as the precision of the model throughout the rest of this paper. A definition of an optimal value for Δ should be defined from the precision of the experimental data. We estimated that the precision of our experiments on the values of c_a and c_b was at least equal to 10^{-5} M, and that our precision on the measurements of the pH was at least on the order of 0.05 units of pH. This translates into a precision for $Q_{exp}-\alpha$ better or on the order of 10^{-5} M in the 4–10 pH range. Hence, an optimal fit for our titration data between pH 3.5 and 10 would have a precision on the order of 10^{-5} M and different sets of models leading to precisions in the order of or smaller than 10^{-5} M cannot be meaningfully discriminated. In this paper, we considered that $Q_{exp}=Q_{exp}(pH)$ is a perfect and smooth experimental curve and that our experimental data could help us determine its characteristics. Using gross experimental data to determine the precision of a model would introduce an uncontrolled bias because the position of the data points on the experimental curve is not well controlled. Hence, we decided to select points on the experimental titration curve at equidistant pH values. Using this prescription, it should be noticed that, for a given model, the value of Δ reaches an asymptotic value Δ_∞ when $n\rightarrow\infty$. This occurs when, between two neighboring sampling points, the deviation of the curve $Q_{exp}-Q_{calc}$ from a straight line is much smaller than Δ_∞.

To determine a good fit of the titration data, we selected one point on the experimental titration curve for every half unit of pH between 3.5 and 10, such that n=14. This ensured that the deviation of the "true" curve Q_{exp} from a straight line between two neighboring sampling points was much smaller than 10^{-5} M, which was the order of magnitude of the precision on the experimental curve itself. Δ was minimized with respect to the values of c_i, $p\bar{K}_i$, and $Q_0-\alpha$ using a model with j types of reactive sites (j=1, 2, 3 or 4; i=1, …, j), and considering that ψ_0 was a constant. The minimization was carried out using the scientific software Mathematica® and the function "FindMinimum". This function calculates the value of Δ with the initial input values and looks for the local minimum, which is reached by following the path of the steepest slope for the decrease of the value of Δ (Wolfram, 1997). The optimization of the model was also performed with the software FITEQL 2.0® and it led to results similar to those obtained with Mathematica® (data not shown), but, with FITEQL 2.0, $Q_0-\alpha$ needed to be introduced as an entry parameter (Westall, 1982).

2.5.2. Modeling of the Fe(II) adsorption isotherms

It is convenient to introduce for each site:

$$x_i = \frac{\bar{T}_i}{2}\left(1 + \frac{[H^+]}{\bar{K}_i}\right) = \frac{10^{-p\bar{T}_i}}{2}\left(10^{-p\bar{T}_i} + 10^{-pH}\right) \quad (9)$$

Then, the concentration of ferrous ions is a solution of the following polynomial equation of order m+1:

$$\left[Fe^{2+}\right]_{calc} = \frac{c_0}{1 + c_{bact} \sum_{i=1}^{m} \frac{c_i}{2x_i + \left[Fe^{2+}\right]_{calc}}} \quad (10)$$

where c_0 is the introduced concentration of ferrous ions. The concentration of ferrous ions adsorbed on the sites of type i, is equal to:

$$\left[Fe^{2+}\right]^{i}_{calc} = \frac{c_0 c_{bact} \left(\frac{c_i}{2x_i + \left[Fe^{2+}\right]_{calc}} \right)}{1 + c_{bact} \sum_{j=1}^{m} \frac{c_j}{2x_j + \left[Fe^{2+}\right]_{calc}}} \quad (11)$$

For a one-site model, Eq. (10) can be analytically solved, which yields:

$$\left[Fe^{2+}\right]_{ads} = \left(\frac{c_0 + c_{bact}c_1}{2} + x_1 \right) - \sqrt{\left(\frac{c_0 - c_{bact}c_1}{2} \right)^2 + x_1(c_0 + c_{bact}c_1) + x_1^2} \quad (12)$$

In an adsorption isotherm, the pH is varied. Increasing the pH results in a decrease of the values x_i and in an increase of adsorption of the ferrous ions. The error of a model with n data points can be measured by:

$$\Delta = \sqrt{\sum_{i=1}^{n} \frac{\left(\left[Fe^{2+}\right]_{calc} - \left[Fe^{2+}\right]_{exp} \right)^2}{n}} \quad (13)$$

where $[Fe^{2+}]_{exp}$ is the concentration of ferrous ions in the aqueous phase, as obtained from the experimental adsorption isotherm. As in Eq. (8), Δ has the dimension of a concentration and is a direct measure of the precision of the model. We estimated that the precision on our experimental data for $[Fe^{2+}]_{exp}$ was on the order of 2×10^{-6} M. In this study, we thus defined optimal fits as those with a precision smaller than 2 μM. To determine a good fit of the experimental data, we selected for each adsorption isotherms 14 points evenly spread at intervals of 0.3 units of pH between pH 3 and pH 6.9. This ensured that the deviation from a straight line of the experimental adsorption isotherm between two sampling points was much smaller than the precision of the experimental data, i.e., about 2 μM. The best fits were obtained by minimizing Δ. We also minimized the precision obtained when the data points from either two or the three adsorption isotherms were taken into account (n=14×2=28 or n=14×3=42). In this paper, we considered one- or two-site models, and assumed that ψ_0 was a constant. We performed the optimization of the modeling parameters with the Mathematica® software, as for the modeling of the titration curve. The optimization of the model was also performed with the software FITEQL 2.0® and it led to results similar to those obtained with Mathematica® (data not shown).

3. Results and discussion

3.1. Batch titration of B. subtilis cells

The acid–base titration of the *B. subtilis* suspension was performed with a cell concentration of 570 mg/l in 10^{-3} M NaCl. On Fig. 1, $Q_{exp}-\alpha$ is plotted as a function of pH. It can be seen that the surface of the

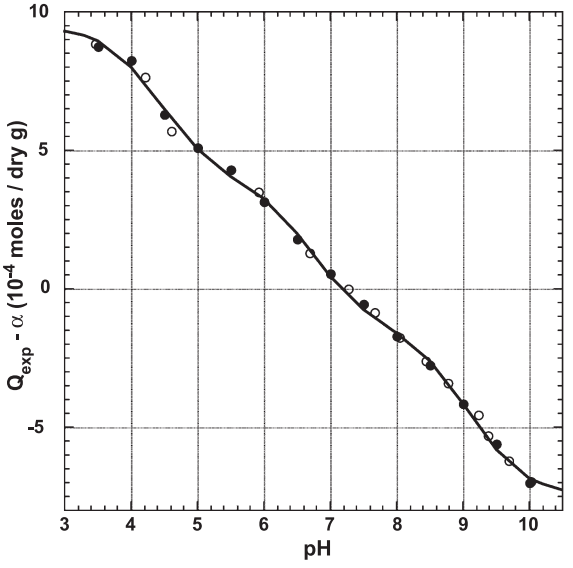

Fig. 1. Anaerobic batch titration of a bacterial suspension at 570 mg/l in 10^{-3} M NaCl: experimental data (○), data selected for the modeling analysis (●), and prediction of the fit using the parameters shown in bold characters in Table 1 (—).

cells becomes more negative as the pH increases, which is expected for bacterial cells (Achouak et al., 1994; Mozes et al., 1991). At pH 3.5, Fig. 1 indicates that $Q_{exp}-\alpha$ was equal to about 9×10^{-4} mol per dry g of bacteria (mol/g in the following). At pH 10.0, $Q_{exp}-\alpha$ was equal to about -7×10^{-4} mol/g. Hence, our titration data indicated that the total concentration of sites, which deprotonate between pH 3.5 and 10.0, was on the order of 16×10^{-4} mol/g. Assuming that the bacteria had a cylindrical shape with a radius R and a length L, a density ρ equal to 1 kg/l, and a dry weight equal to X% of their full weight, the geometric surface area σ of the cells was equal to $(2/(\rho X))(R+L)/(RL)$, where the lengths are expressed in μm. Using X=0.2 and $(R+L)/(RL)$=3 (e.g., R=0.3 and L=3), this leads to a surface area σ=30 m^2/g. The surface concentration of sites present on the bacterial surfaces was thus on the order of three sites per 0.1 nm^2. This is quite high and it suggests that the surfaces were at least slightly penetrable for the protons, so that some reactive sites inside the outer part of the cell wall were accessible through the titration. Such a high density of proton-reactive sites is consistent with other titration studies of *B. subtilis*, where the concentrations obtained for reactive sites are highly variable but within the range $10–100\times10^{-4}$ mol/g (Daughney and Fein, 1998; Daughney et al., 2001; Fein et al., 1997).

The minimization of Δ could lead to values smaller than 10^{-5} M, the precision of the experimental data, only if at least three types of sites were invoked. This is consistent with previous studies (Daughney and Fein, 1998; Daughney et al., 2001; Fein et al., 1997). An optimal fit for the whole titration curve is shown on Fig. 1 as a line. The first type of sites was characterized by a $p\bar{K}$ value $p\bar{K}_1$=4.45 and a concentration $c_1=5.6\times10^{-4}$ mol/g (Table 1). A value of 6.74 and a concentration $c_2=5.3\times10^{-4}$ mol/g could be associated to the second type of sites. Finally, the third type of sites had a $p\bar{K}$ value of 9.08 and a concentration $c_3=6.1\times10^{-4}$ mol/g. The value of $Q_0-\alpha$ was equal to 9.5×10^{-4} mol/g. As explained in Section 2.5.1, $Q_0-\alpha$ is an adjustable parameter which does not carry any information by itself on the characteristics of the reactive sites.

In our modeling analysis, we did not attempt to take into account the dependence of the electrostatic potential on the bacterial surfaces with the pH. Proper modeling of the electrostatic effects onto and in bacterial cell walls is still a matter of current research (Martinez et al., 2002). However, considering that ψ_0 had a constant value is a first reasonable approximation. Recent measurements have shown that the electrophoretic mobility of *B. subtilis* ATCC 168 cells at a low ionic strength does not vary much above pH 3 and is on the order of $-2.75\pm0.50\times10^{-8}$ m^2 V^{-1} s^{-1} (Okuda et al., 2003). This relative stability of the electrophoretic mobility as the pH increases although the cell walls undergo deprotonation could be related to a condensation of the counter-ions in the cell walls, occurring once the electrostatic potential is strong enough to sequestrate them in the vicinity of the deprotonated groups. Using the Schmoluchowski equation (Mozes et al., 1991), and assuming that the zeta potential can be used to estimate ψ_0, this suggests that the zeta potential is equal to -35 ± 7 mV, and that $\psi_0\approx-0.38\pm0.07$. Using ψ_0=0 or ψ_0=−0.38, our modeling analysis suggests that the reactive sites for the protons had pK values of 4.45, 6.74 and 9.08, or 4.07, 6.36, and 8.70, respectively.

It should be noted that, although this set of parameters led to a good prediction of the titration curve, there were other sets of parameters with slightly different values, which led to fits with a comparable precision. Hence, we estimate that the accuracy on the parameters of the model achieved through the minimization was on the order of

Table 1
Parameters characterizing various fits obtained for the titration curve of *B. subtilis*

Precision of the fit Δ (10^{-5} M)	$Q_0-\alpha$ (Section 2.5.1)	Concentrations of the various types of sites (10^{-4} mol/dry g of bacteria)				$p\bar{K}$ values of the various types of sites ($p\bar{K}=pK-\psi_0$)			
		c_1	c_2	$c_{2'}$	c_3	$p\bar{K}_1$	$p\bar{K}_2$	$p\bar{K}_{2'}$	$p\bar{K}_3$
0.96	**9.5**	**5.6**	**5.3**	**X**	**6.1**	**4.45**	**6.74**	**X**	**9.08**
1.16	9.5	5.6	2.6	2.8	6.1	4.45	6.20	7.30	9.08
0.69	9.6	5.0	3.7	3.3	5.5	4.31	6.16	7.55	9.31
0.71	9.5	5.4	3.5	2.9	5.6	4.42	6.40	7.53	9.30

0.2×10^{-4} mol/g for the concentrations c_i and 0.2 units of pH for the $p\bar{K}_i$ values. The three-site model reproduced the titration curve, but there were possibly additional sites. However, we could not distinguish between them from our titration data. Various kinds of sites were possibly pooled together with an intermediate value for the $p\bar{K}$ in our fits. For instance, an almost equivalently good fit could be obtained by replacing the second site by a site $2'$ with a concentration $c_{2'}=2.6\times10^{-4}$ mol/g and $p\bar{K}_{2'}=6.20$, and a site $2''$ with $c_{2''}=2.8\times10^{-4}$ mol/g and $p\bar{K}_{2''}=7.30$, as shown in Table 1. For these reasons, it has been debated in recent years whether one should try to fit a titration curve with a minimal number of sites or with a spectral approach, according to which the density of concentration of sites for every possible p*K* value would be evaluated (Fein et al., 1997; Martinez and Ferris, 2001; Martinez et al., 2002). Here, we have chosen the three-site approach here, but one should keep in mind that it may also be interpreted as a rough representation of the spectral approach.

There are indeed many proton-reactive groups in the cell wall of Gram-positive bacterial cells, with p*K* values spanning a large range of values. The structure of the cytoplasmic membrane of *B. subtilis* cells is mainly composed of phosphatidylethanolamine (PE), which accounts for 20–40% of the total amount of phospholipids, phosphatidylglycerol (PG), and diphosphatidyl glycerol (Archibald, 1989; Opekarova and Tanner, 2003; Stryer, 1996). These molecules contain one (PE, PG) or two (di-PG) phosphodiester groups, with p*K* values in the 1–3 range, and PE contains also an amino group with a p*K* value in the 10–11 range (Marsh, 1990). The structure of the cell walls is made of peptidoglycan (Archibald, 1989; Mozes et al., 1991), which possesses many carboxylic and amino groups. In the peptidoglycan of *B. subtilis*, the second carboxylic group of the meso-diaminopimelic acids is amidated, some of the terminal D-alanine amino acids of the side chains are removed, and the degree of crosslinking is about 45±15%, so that there are one to two carboxylic group and zero to one amino group per monomer of the glycan chains (Archibald, 1989). The cell walls also contain lipoteichoic, teichoic, and possibly teichuronic acids. The teichoic and the lipoteichoic acids are polymers, each monomer containing one phosphodiester group with a p*K* value in the 1–2 range and in most cases one amino group, present through the alanine amino acid attached to the polymer backbone by the ester bond, with a p*K* likely on the order of 10 (Archibald, 1989; Stryer, 1996). Teichuronic acids appear mainly when under phosphate limitation and contain carboxylic groups (Mozes et al., 1991). The cell walls and membranes of *B. subtilis* also contain some proteins, likely carrying carboxylic (aspartic, glutamic acid, and cysteine with values of p*K*=3.9, 4.3, and 8.3, respectively) and basic groups (lysine, tyrosine, arginine, and histidine with values of p*K*=10.8, 10.9, 12.5, and 6.0, respectively). Finally, hydroxyl groups are present in various of the molecules discussed here, and are believed to have a p*K* value equal to or larger than 10 (Stryer, 1996).

Our titration data indicates, as shown in previous studies, that the bacteria have a strong buffering capacity throughout the pH range tested here, i.e., from pH 3 to 10. The sites of type 1, with a p*K* value around 4.0–4.5, have been tentatively assigned to carboxylic groups, while the sites with high p*K* as have been interpreted as amino or hydroxyl groups, and the sites with intermediate p*K* as have been related to phosphoryl groups (Fein et al., 1997, 2001; Ngwenya et al., 2003). However, in our view, caution should be exercised with such interpretations. As explained above, the cell walls and the membranes of *B. subtilis* cells may contain few reactive sites with p*K* values in the 3–10 range. Apart from the carboxylic groups, we would expect that most reactive sites have p*K* values lower than 3, in the case of the numerous phosphodiester groups, or larger than 10, in the case of most amino and hydroxyl groups. It is possible that the p*K* values of these groups are different when they are inside the cell wall structure from what they are when the sites are exposed to the bulk aqueous solution. However, because we do not know how to estimate these possible variations, we will refer, for the remainder of this paper, to the reactive sites that we detected in our titration data as sites 1, 2, and 3.

3.2. Adsorption kinetics

One of the important variables, which need to be considered, when adsorption of a molecule on bacterial cells is studied, is the equilibration time. It

must be long enough that adsorption can proceed and possibly reach some kind of equilibrium. However, at longer time scales, the danger that bacteria will degrade or change becomes larger. There is also a possibility that a slower process of absorption will be superimposed on the process of adsorption. We observed that the adsorption of ferrous ions onto bacterial cells was a rather quick process. Fig. 2a displays the percentage of adsorbed Fe(II) and the equilibrium pH after different equilibration times for two different initial pH conditions: one neutral condition (pH_{init}=7.3) and one acidic condition (pH_{init}=5.0). In both cases, it can be seen that, after 1 min, a large portion of Fe(II) was already adsorbed, although the pH and the fraction of adsorbed Fe(II) drifted significantly during the following minutes. After 20–30 min at neutral pH and after about 60 min in the acidic system, pH and adsorbed Fe(II) variations could still be observed, but they were slow, as shown in Fig. 2a (on this figure, the time is plotted on a logarithmic scale). The slow decrease of adsorbed Fe(II) observed in the acidic system over long equilibration times is not surprising, as the aging of the cells likely leads to an increase of the concentration of dissolved organic ligands, which may be able to retain some of the Fe(II) in the dissolved phase. In the acidic system where equilibrium was longer to achieve, it should also be noted that the drift of pH and adsorbed Fe(II) seemed to be correlated. As the pH increased over time, the fraction of adsorbed Fe(II) increased as well. This is consistent with the fact that when the pH increases, bacterial cell surfaces become more attractive towards metallic cations (Daughney and Fein, 1998). Hence, the equilibration time needed to obtain an adsorption isotherm at equilibrium was possibly smaller than that needed to obtain equilibrium for a given sample. As a result, we performed full adsorption isotherms using equilibration times of 10, 30, and 60 min. The reproducibility of the results was robust, as three isotherms realized independently with an equilibration time of 30 min almost perfectly overlapped. The results, which are shown on Fig. 2b, indicate that the three isotherms converged at low pH, but that the isotherm obtained after just 10 min of equilibration indicated a slightly lower rate of adsorption of the Fe(II) than at neutral pHs. There was very little difference between the isotherms obtained after 30

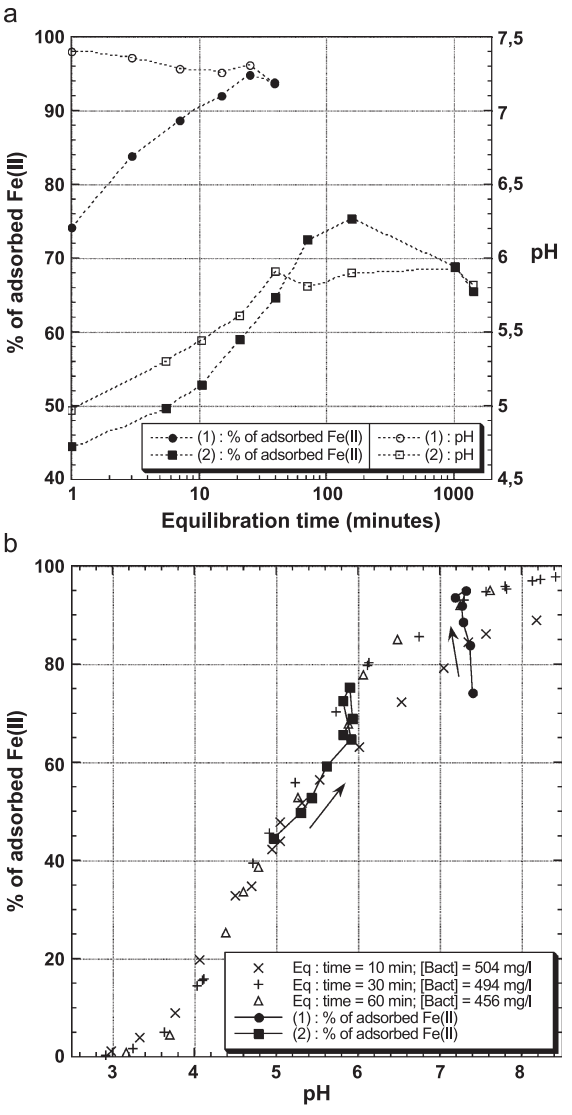

Fig. 2. (a) Kinetics in an adsorption experiment of 10^{-4} M Fe(II) onto a 500 mg/l *Bacillus subtilis* suspension at two different pH ranges: percent (%) of adsorbed Fe^{2+} (full symbols) and pH (open symbols) as a function of the equilibration time for suspension A (494 mg/l; ●, ○) and suspension B (510 mg/l; ■, □). (b) Adsorption isotherms realized for an equilibration time of 10 min ("x" crosses, suspension at 504 mg/l), 30 min ("+" crosses, suspension at 494 mg/l), and 60 min (△, suspension at 456 mg/l). The measurements presented in panel a are also presented in panel b in full symbols; arrows point towards longer equilibration times (● and ■ as in panel a).

and 60 min. The results shown on Fig. 2a are replotted on Fig. 2b. The arrows indicate the direction of time. At low pH conditions, the measurements fell onto the adsorption isotherms even after an equilibrium time of

just 1 min. At neutral pH, it took about 10–20 min before an agreement between the measurements for a sample and the isotherms at 30 or 60 min was reached. Altogether, these results suggest that an equilibration time of 60 min is adequate for the realization of an adsorption isotherm. This is consistent with previous studies, which examined the adsorption of metallic cations onto bacterial cells (Fein et al., 1997; Martinez and Ferris, 2001; Ngwenya et al., 2003).

3.3. Adsorption isotherms

3.3.1. Experimental adsorption/desorption isotherms: qualitative and semiquantitative analysis

The adsorption isotherms of Fe(II) onto *B. subtilis*, are shown on Fig. 3a for bacterial concentrations of 50 mg/l, 500 mg/l, and 5 g/l. The desorption isotherm obtained at a bacterial concentration of 500 mg/l is also shown on Fig. 3a. It overlaps with the adsorption isotherm obtained at the same bacterial concentration. This indicates that the amount of Fe(II), which was absorbed by the cells or irreversibly adsorbed onto their surfaces, could be neglected. Therefore, it can be considered that the adsorption isotherms presented on Fig. 3a describe a situation of equilibrium. The three adsorption isotherms indicate that adsorption increased with pH, as expected from Eq. (10). This increase of adsorption was likely due to the lesser competition of the protons for the reactive sites at higher pH, and possibly also to some extent to the decrease of the surface charge of the bacterial cells, which are usually positively charged or neutral at low pH and negatively charged at neutral or basic pH (Mozes et al., 1991). An interesting feature of the adsorption isotherm is that adsorption of the ferrous ions decreased above pH 9–9.5 (Fig. 3b). This was likely because, above pH 9, an increasing fraction of the dissolved ferrous ions was complexed with three hydroxide ions (Langmuir, 1997). The affinity of the ferrous ions was possibly higher for the hydroxide ions than for the bacterial surfaces at high pH. In addition, the complexation of the ferrous ions with the hydroxide ions reversed the charge of the ferrous ions. As a result, at high pH, the ferrous ions were repelled by the bacterial surfaces because both were negatively charged. Although this phenomenon appeared clearly, we did not attempt to model it quantitatively, because, above pH 7–8, adsorption of the ferrous ions on the

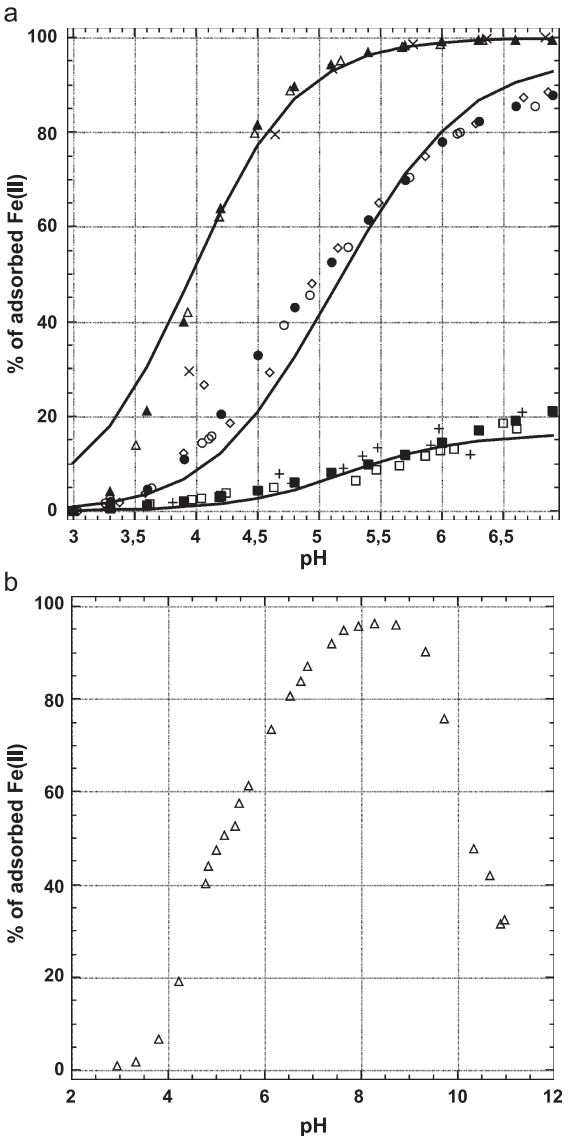

Fig. 3. (a) Adsorption isotherms realized for an equilibration time of 60 min and bacterial suspensions at 47.0 mg/l (□), 48.8 mg/l ("+" crosses), 456 mg/l (○), 4.59 g/l ("x" crosses), and 5.30 g/l (△) and desorption isotherm for a bacterial suspension at 522 mg/l (◇). The data selected for the modeling analysis is also shown for 48 mg/l (■), 456 mg/l (●), and 5.3 g/l (▲). The prediction of the one-site model with $p\bar{K}=6.74$, $c=3.5\times10^{-4}$ mol/g, and $p\bar{T}'=-1.22$ is shown as lines, for 48 mg/l, 456 mg/l, and 5.3 g/l. (b) Adsorption isotherm realized for an equilibration time of 30 min and a bacterial suspension at 510 mg/l (△). The decrease of the Fe(II) adsorbed amount occurs clearly above pH 9.

glassware used in the experiment also became significant. Consequently, the values obtained for the fraction of adsorbed ferrous ions using our protocol were overestimated at high pH. The adsorption isotherms presented in Fig. 3a are thus limited to a pH range of 3–7. This range covers the conditions found in many natural aquatic systems.

As can be expected, adsorption of the ferrous ions was larger when the concentration of bacteria increased at a given pH. The Langmuir isotherm at neutral pH for a bacterial concentration of 500 mg/l is shown on Fig. 4. In a Langmuir isotherm, the limit $c_0 \rightarrow \infty$ is probed at a constant pH and at a constant bacterial concentration. From Eqs. (10)–(11), it is easily shown that the adsorbed concentration of ferrous ions in this limit is equal to $c_{\text{bact}} \sum_{i=1}^{m} c_i$. Hence, a Langmuir isotherm at a sufficiently high pH and reaching sufficiently high values of c_0 ($c_0 \gg x_i$) provides a good way to estimate the concentration of adsorbing sites. The precision of our experimental data for the Langmuir isotherm was not as good as for the adsorption isotherms shown in Fig. 3a. This is due to various reasons such as the difficulty to fix the pH at a constant value without adding a buffer. However, it can clearly be seen in Fig. 4 that the slope of the isotherm is high up to a concentration of dissolved ferrous ions of approximately 10^{-4} M, and that it decreases quickly at higher dissolved Fe(II) concentrations. The Langmuir isotherm in Fig. 4 also suggests that the concentration of reactive sites available on the bacterial surfaces for the ferrous ions was equal to roughly 3.5×10^{-4} mol/g which is much lower than what was suggested by the titration data. In a study by Kulczycki et al. (2002) on the adsorption of lead and cadmium onto *B. subtilis* cells grown in exponential phase, the concentration of sites available for adsorption of Cd^{2+} was estimated to be equal to 3.6×10^{-4} mol/g which is in agreement with our own estimate for Fe^{2+}, whereas the concentration of sites available for Pb^{2+} was slightly lower, i.e., 2.7×10^{-4} mol/g. Three previous studies (Liu et al., 2001; Roden and Urrutia, 2002; Urrutia and Roden, 1998) have used a Langmuir isotherm to describe the adsorption of ferrous ions onto *Shewanella putrefaciens* CN32, *Shewanella alga* BrY, and *Geobacter metallireducens* which are Gram-negative bacteria (Lovley, 2000). These studies obtained slightly lower concentrations of reactive sites, as expected for Gram-negative cells (Martinez and Ferris, 2001), i.e., on the order of 1–2×10^{-4} mol/g. Assuming that the surface area of the bacteria was equal to 30 m^2/g (see Section 3.1), the concentration of reactive sites for the ferrous ions (i.e., 3.5×10^{-4} mol/g) should be equivalent to about 0.7 sites per 0.1 nm^2. This corresponds to a high packing density of the Fe(II) on the bacterial surfaces, but it also indicates that the Fe(II) did not necessarily penetrate the cell walls, unlike the protons (Section 3.1).

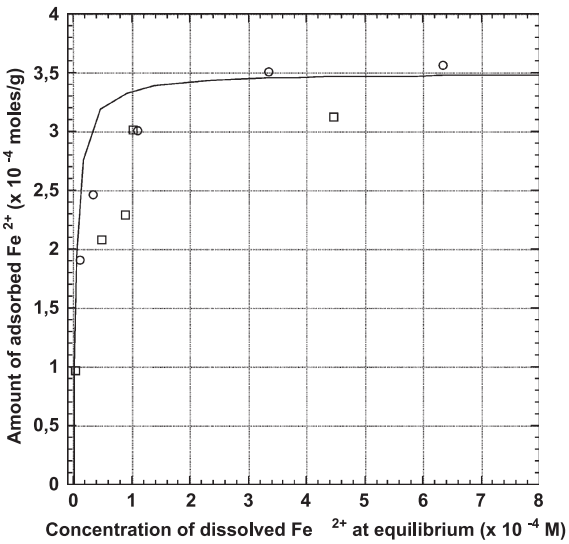

Fig. 4. Langmuir isotherm realized at pH=7.0±0.5 for a suspension at 470 (○) and 488 mg/l (□). The prediction of the one-site model with $p\bar{K}$=6.74, c=3.5×10^{-4} mol/g, and $p\bar{T}'$=−1.22 is shown as a line for a suspension at 480 mg/l and at pH 7.0.

The adsorption isotherm at 50 mg/l corresponded to the conditions where the bacterial surfaces were saturated ($[Fe^{2+}] \approx c_0$), and, according to the result of the Langmuir isotherm, to the situation where $c_{\text{bact}} \sum_{i=1}^{m} c_i < c_0$. For this isotherm, Eq. (11) may be approximated by its limit when $c_{\text{bact}} \rightarrow 0$:

$$\left[Fe^{2+}\right]_{\text{calc}}^{i} = c_i c_{\text{bact}} \left(\frac{c_0}{2x_i + c_0} \right) \tag{14}$$

Eq. (14) indicates that for the adsorption isotherm of a bacterial suspension at a low concentration, the onset of adsorption for a site i occurs when $2x_i \approx c_0$. Neglecting the dependency of ψ_0 with the pH, the main dependency of x_i with the concentration of protons is linear, and x_i decreases when the pH

increases, from ∞ down to its minimal value equal to $\bar{T}_i$ when pH>p$\bar{K}_i$ (see Eq. (9)). If $c_0 \ll \bar{T}_i$, adsorption onto site i is negligible, even at high pHs. If $c_0 \approx \bar{T}_i$, some adsorption can occur for pH≥p$\bar{K}_i$. If $c_0 \gg \bar{T}_i$, i.e., if pc_0−p$\bar{T}_i$, where pc_0=−log$_{10}$(c_0), most sites i can be occupied by ferrous ions at high pH and the onset of adsorption onto the sites i occurs for:

$$\mathrm{pH} \approx \mathrm{pH}_i = \mathrm{p}c_0 - \mathrm{p}\bar{T}_i' \tag{15}$$

For an adsorption isotherm at a low bacterial concentration, the adsorption edge occurs over the range covered by the pH$_i$ values. The extent of adsorption depends on the bacterial concentration, but the width and the location of the adsorption edge are independent of it. The adsorption edge of the isotherm at a bacterial concentration of 50 mg/l was quite wide and was located at about pH=5.5±1.0. Using Eq. (15), this suggests that the adsorption constant of the active sites was on the order of $\mathrm{p}\bar{T}_i' \approx -1.5 \pm 1.0$, leading to $\mathrm{p}\bar{T}_i' \approx -1.5 \pm 1.0$ or $\mathrm{p}\bar{T}_i' \approx -1.9 \pm 1.0$ using ψ_0=0 or ψ_0=−0.38, respectively (see Section 3.1). Above pH 6–6.5, the amount of ferrous ions adsorbed onto the bacteria was close to 3.5×10^{-4} mol/g, the maximal value predicted by the Langmuir isotherm. This suggests that, for most of the active sites, the onset of adsorption occurred for a pH significantly lower than p$\bar{K}_i$ ($c_0 \gg \bar{T}_i$, pH$_i$<p$\bar{K}_i$). The p$\bar{K}$ value of most of the active sites was thus likely higher than 4.5, leading to pK>4.5 using ψ_0=0, or pK>4.1, using ψ_0=−0.38.

If we now look at the limit of high bacterial concentrations, and assume that for each site i $c_0 \ll c_{\mathrm{bact}} c_i$, it is easily shown self-consistently that $[\mathrm{Fe}^{2+}] \ll 2x_i$ and that Eq. (11) can be rewritten as:

$$[\mathrm{Fe}^{2+}]^i_{\mathrm{calc}} = c_0 \frac{c_{\mathrm{bact}} c_i}{2x_i + c_{\mathrm{bact}} c_i + \sum_{j\neq i,\ j=1}^{m} \left(c_{\mathrm{bact}} c_j \frac{x_i}{x_j} \right)} \tag{16}$$

As long as $2x_i \gg c_i c_{\mathrm{bact}}$ for all i, adsorption of the ferrous ions is negligible. However, as soon as there is at least one site such that $2x_i \ll c_i c_{\mathrm{bact}}$, adsorption is almost complete. It seems reasonable to assume that Eq. (16) is a good approximation for the adsorption isotherm at 5 g/l, where the total concentration of reactive sites, as estimated from the Langmuir isotherm, was on the order of 17.5 c_0. We have also shown, from the examination of the isotherm at 50 mg/l that $c_0 \gg \bar{T}_i$ for most sites. The pH value at which $2x_i \approx c_i c_{\mathrm{bact}}$ is thus much lower than p$\bar{K}_i$ for these sites, and it is then given by:

$$\mathrm{pH} \approx \mathrm{pH}_i' = \mathrm{p}c_{\mathrm{bact}} + \mathrm{p}c_i - \mathrm{p}\bar{T}_i' \tag{17}$$

The adsorption edge for an adsorption isotherm at large bacterial concentrations is given by the lowest value for pH$_i'$. The extent of adsorption and the width of the adsorption edge are then independent on the bacterial concentration, but the location of the adsorption edge decreases by one unit of pH when the bacterial concentration increases by a factor 10. Because the adsorption edge is controlled by the first site onto which adsorption occurs, its width is limited and independent on the number of active sites, which can potentially become successively dominant as the pH increases. This qualitative observation is in agreement with our experimental results which indicate that the width of the adsorption edge decreased when the bacterial concentration increased (Fig. 3a). The adsorption edge was located at pH=4.2±0.7 for the isotherm at 5g/l (pc_{bact}=−log$_{10}$(c_{bact})=−0.70). This suggests that the p$\bar{K}$ value of most reactive sites was much larger than 4.2, i.e., pK>4.2, using ψ_0=0, or pK>3.8, using ψ_0=−0.38 (see Section 3.1). In addition, if we consider that there was only one kind of sites, with a concentration $c_1=3.5\times10^{-4}$ mol/g (pc_1=−log$_{10}$(c_1)=3.45), the corresponding adsorption constants can be estimated as equal to $\mathrm{p}\bar{T}_i' \approx -1.45 \pm 0.35$, leading to $\mathrm{p}\bar{T}_i' \approx -1.45 \pm 0.35$ or to $\mathrm{p}\bar{T}_i' \approx -1.85 \pm 0.35$ using ψ_0=0 or ψ_0=−0.38, respectively, which is in excellent agreement with our estimate obtained from the observation of the isotherm at 50 mg/l. If we consider that there were more than one type of sites, a less-negative value for p$\bar{T}_i'$ is obtained for the first active site using Eq. (17).

The adsorption isotherm at 500 mg/l corresponded to the intermediate case where $c_{\mathrm{bact}} \sum_{i=1}^{m} c_i > c_0$ and $c_{\mathrm{bact}} \sum_{i=1}^{m} c_i = 0(c_0)$. In this situation, reactive sites contributing to the adsorption edge are such that $c_i c_{\mathrm{bact}} \approx c_0$, and the onset of adsorption for these sites occurs when $2x_i \approx c_i c_{\mathrm{bact}} \approx c_0$. Hence, both Eqs. (15) and (17) are correct. The adsorption was located at pH=5.0±1.0 for the

isotherm at 500 mg/l (Fig. 3a), i.e., at about one unit of pH more than for the isotherm at 5 g/l, which is in agreement with Eq. (17). As a result, the values of $p\bar{T}_i$, as estimated by examining the isotherm at 500 mg/l, are on the same order of magnitude as when examining the isotherm at 5 g/l.

An interesting aspect of Eqs. (15) and (17) and of our semi-quantitative analysis of our experimental adsorption isotherms is that they clearly demonstrate that the adsorption edge in an adsorption isotherm is never located at pH values much larger than the pK of the corresponding active sites. Instead, it is usually located at significantly lower values. For a given site, the maximal pH value where the onset of adsorption can occur is $p\bar{K}_i$, and this situation occurs only when $c_0 \leq c_i c_{bact} \approx \bar{T}_i$ or when $c_i c_{bact} \leq c_0 \approx \bar{T}_i$. If $c_0 \leq c_i c_{bact} \ll \bar{T}_i$ or $c_i c_{bact} \leq c_0 \ll \bar{T}_i 10^{2\psi 0}$, the site can be ignored as no significant adsorption occurs. In addition, if $\bar{T}_i \ll c_i c_{bact}$ or $\bar{T}_i \ll c_0$, the onset of adsorption occurs at a pH value much smaller than $p\bar{K}_i$, which is thus likely significantly smaller than pK_i. In general, the location of the adsorption edge of an isotherm should thus certainly not been used as an indicator of the pK value of the reactive sites, but rather as a lower boundary for these sites. There is absolutely no need for a reactive site to be deprotonated before adsorption of a competitive ion can occur. This seems to be often misunderstood, as isotherms similar to our isotherm at 5g/l are sometimes interpreted by mentioning that the metal ions adsorb on the reactive sites once those are deprotonated and by proposing that an adsorption edge at a pK value of 4 indicates that adsorption occurs mainly on the carboxylic groups.

3.3.2. Modeling of the adsorption data: one-site model

We modeled each adsorption isotherm using a one-site model. For the adsorption isotherms at 50 and 500 mg/l, optimal fits with a precision Δ<2 μM could be obtained for a wide range of parameters. However, we could not obtain any optimal fit using a $p\bar{K}$ value lower than 4.93 (50 mg/l) or 5.97 (500 mg/l), a concentration lower than 3.4×10^{-4} mol/g (50 mg/l) or outside of the range $1.9–3.1\times10^{-4}$ mol/g (500 mg/l), or a $p\bar{T}'$ adsorption constant larger than −0.81 (50 mg/l) or outside of the range [−0.91;−0.56] (500 mg/l). The range of the parameters leading to a precision lower than 3 μM are shown on Fig. 5, for a site concentration fixed at 3.5×10^{-4} mol/g. The best fits obtained assuming that the adsorption was taking place either on the type 2 sites ($p\bar{K}$=6.74) or on the type 3 sites ($p\bar{K}$=9.08) are shown in Table 2 for both isotherms. Using a site concentration equal to 3.5×10^{-4} mol/g, the best fit obtained for the adsorption isotherm at 500 mg/l is also shown, as well as the best fits obtained for both adsorption isotherms (50 and 500 mg/l) with a $p\bar{K}$ value of 6.74. For the adsorption isotherm at 5 g/l, no optimal fit could be obtained. The best fits that we could generate had a precision Δ close to 4.9–5.0 μM. We could not obtain any fit with a precision lower than 6.0 μM using a $p\bar{K}$ value lower than 5.44, a concentration lower 5.5×10^{-5} mol/g, or a $p\bar{T}'$ value larger than −0.42. The range of parameters leading to fits with a precision lower than 6.0 μM is shown on Fig. 5c using a site concentration equal to 3.5×10^{-4} mol/g. The best fits obtained assuming that the adsorption was taking place either on the type 2 sites ($p\bar{K}$=6.74) or on the type 3 sites ($p\bar{K}$=9.08), and using a site concentration of 3.5×10^{-4} mol/g or the site concentration given by the titration data, are shown in Table 2. Modeling both isotherms at 50 and 500 mg/l together, the best fit was obtained for a $p\bar{K}$ value of 5.83 and an adsorption constant $p\bar{T}'$ equal to −1.13 (see Table 3), which led to an average precision of 2.03 μM (Table 3). We could not obtain any fit with a precision lower than 3 μM using a $p\bar{K}$ value outside of the range 5.46–6.48, a concentration outside of the range $2.5–9.8\times10^{-4}$ mol/g, or a $p\bar{T}_i$ adsorption outside of the range [−1.51; −0.76]. For a site concentration of 3.5×10^{-4} mol/g for instance, the models leading to a precision lower than 3 μM are shown on Fig. 5d. When we modeled all three adsorption isotherms together, the "best fit" we could obtain corresponded to a $p\bar{K}$ value of 6.16, a site concentration of 5.2×10^{-4} mol/g, a $p\bar{T}'$ value of −1.39, and a precision Δ=4.47 μM (Table 3). Fits with a precision lower than 6 μM could not be obtained using a $p\bar{K}$ value lower than 5.45, a concentration lower than 2.1×10^{-4} mol/g or a $p\bar{T}'$ value larger than −0.89. The models using a site concentration of 3.5×10^{-4} mol/g and leading to a precision lower than 6 μM are shown on Fig. 5e. The best fit compatible with the Langmuir isotherm,

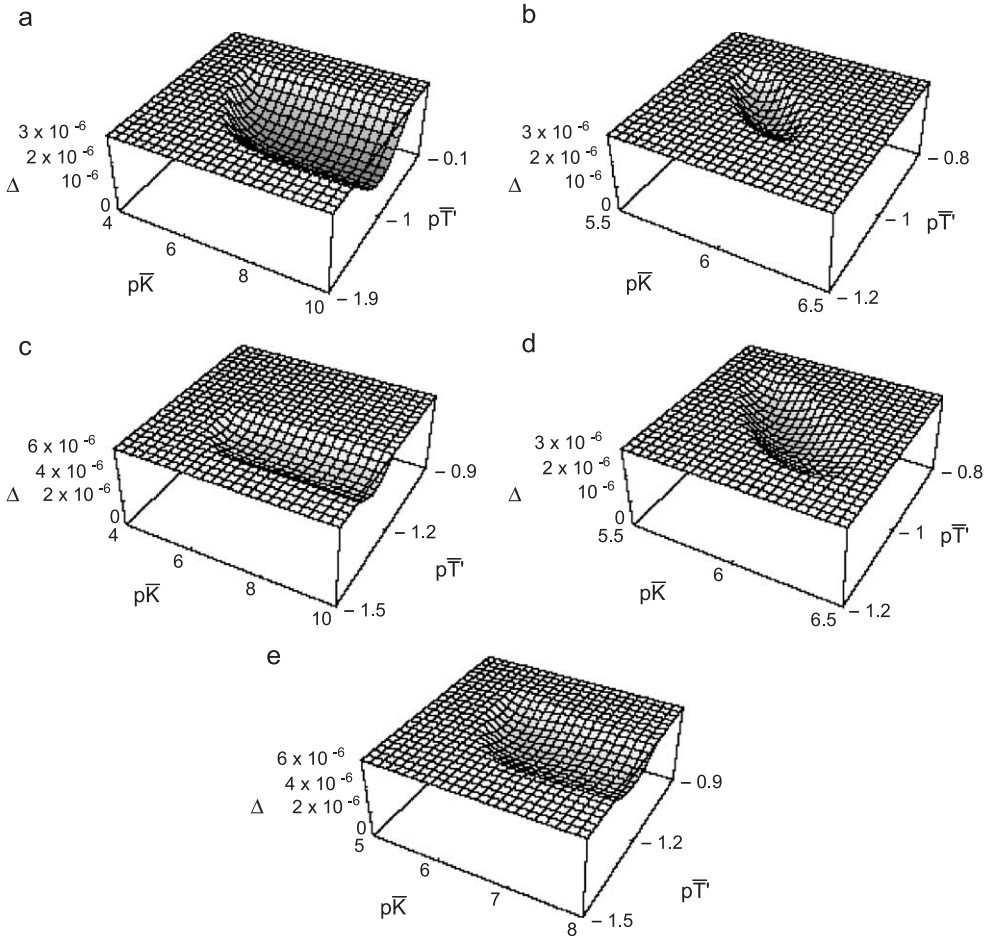

Fig. 5. Precision Δ as a function of the p$\bar{K}$ and p$\bar{T}'$ values for a site concentration of 3.5×10^{-4} mol/g for the adsorption isotherm at 48 mg/l (a), 456 mg/l (b), and 5.3 g/l (c), both isotherms at 48 and 456 mg/l (d) and all three isotherms (e). The flat regions correspond to pairs of parameters, which lead to a precision larger than the upper limit of the z-axis, as indicated in each figure. The depressions correspond to precisions lower than this upper limit.

i.e., with a site concentration of 3.5×10^{-4} mol/g, was characterized by a pK value of 6.40, a p$\bar{T}'$ value of −1.20, and a precision Δ=4.75 μM (Table 3). This fit was compatible with the titration data, but a fourth site needed to be invoked to properly model the titration curve (Table 1). Using instead a p$\bar{K}$ value equal to 6.74 or to 9.08, as suggested by the modeling of the titration data (Section 3.1), the best fit was obtained in both cases for a value equal to −1.22, which led to Δ=4.85 μM or to Δ=5.14 μM for p$\bar{K}$=6.74 and 9.08, respectively (see Table 3). The fit obtained using p$\bar{K}$=6.74 is shown on Figs. 3a and 4. It is instructive to note that the optimal p$\bar{T}'$ value was almost independent of the p$\bar{K}$ value. In addition, it changed only relatively slowly with the site concentration. For instance, if a site concentration of 5.3×10^{-4} mol/g was selected, together with p$\bar{K}$= 6.74, the optimal p$\bar{T}'$ value was shifted by about 0.2 (Table 3), which is on the order of magnitude of the precision on p$\bar{T}'$, as shown by Fig. 5e.

Altogether, the modeling analysis indicated that, rather than a single best fit, there were families of fits, which were equivalent to the described individual adsorption isotherms. Adsorption isotherms at 50 and 500 mg/l could either be fitted individually or fitted together. The range of parameters appropriate to

Table 2
Parameters characterizing various fits obtained for the independently modeled adsorption isotherms (one-site model)

Bacterial concentration of the selected isotherm (dry weight)	Precision of the fit Δ (10^{-6} M)	Concentration of reactive sites (10^{-4} mol/dry g of bacteria)	p$\bar{K}$ value of the reactive sites (p$\bar{K}$=p$K-\psi_0$)	Adsorption constant of the reactive sites (Section 2.5)	
				p$\bar{T}$	p$\bar{T}'$
50 mg/l $-\log(c)$=4.77	1.19[a]	4.08	9.08	7.81	−1.27
	1.20[b]	4.25	6.74	5.45	−1.29
	1.72[c]	3.50	6.74	5.73	−1.01
500 mg/l $-\log(c)$=3.80	1.33[a]	2.03	9.08	8.43	−0.65
	1.37[b]	2.15	6.74	6.05	−0.69
	4.86[c]	3.50	6.74	5.64	−1.10
	2.18[d]	3.50	5.92	4.93	−0.99
5 g/l $-\log(c)$=2.73	5.08[e]	3.50	6.74	5.44	−1.30
	5.04[e]	5.30	6.74	5.26	−1.48
	5.05[f]	3.50	9.08	7.78	−1.30
	4.99[g]	6.10	9.08	7.53	−1.55

[a] Best fit using p$\bar{K}$=9.08.
[b] Best fit using p$\bar{K}$=6.74.
[c] Best fit using p$\bar{K}$=6.74 and a site concentration of 3.5×10^{-4} mol/g.
[d] Best fit using a site concentration of 3.5×10^{-4} mol/g.
[e] Best fit using p$\bar{K}$=6.74 and a site concentration of 5.3×10^{-4} mol/g.
[f] Best fit using p$\bar{K}$=9.08 and a site concentration of 3.5×10^{-4} mol/g.
[g] Best fit using p$\bar{K}$=6.74 and a site concentration of 3.5×10^{-4} mol/g.

describe both adsorption isotherms was relatively well defined. On the other hand, the adsorption isotherm at 5g/l could only be approximately fitted. This was because its shape was too sharp to be described by Eqs. (10)–(11), at least when ψ_0 was considered to be constant. The best fits that we could obtain for all

Table 3
Parameters characterizing various fits obtained from modeling the adsorption isotherms together (one-site model)

Bacterial concentration of the selected isotherm (dry weight)	Precision of the fit Δ (10^{-6} M)	Concentration of reactive sites (10^{-4} mol/dry g of bacteria)	p$\bar{K}$ value of the reactive sites (p$\bar{K}$=p$K-\psi_0$)	Adsorption constant of the reactive sites (Section 2.5)	
				p$\bar{T}$	p$\bar{T}'$
50 and 500 mg/l	2.03[a]	4.53	5.83	4.70	−1.13
	2.24[b]	3.50	5.95	3.42	−0.99
All three isotherms	4.47[c]	5.20	6.16	4.77	−1.39
	4.75[d]	3.50	6.40	5.20	−1.20
	4.80[e]	4.02	6.74	5.45	−1.29
	4.98[f]	5.30	6.74	5.31	−1.43
	4.85[g]	3.50	6.74	5.52	−1.22
	5.14[h]	3.50	9.08	7.86	−1.22

[a] Best fit if only the isotherms at 50 and 500 mg/l are considered Δ=1.49, 2.46, and 10.4 μM for the isotherms at 50 mg/l, 500 mg/l, and 5g/l, respectively.
[b] Best fit if only the isotherms at 50 and 500 mg/l are considered and $c_1=3.5\times10^{-4}$ mol/g Δ=2.27, 2.21, and 11.1 μM for the isotherms at 50 mg/l, 500 mg/l and 5g/l, respectively.
[c] Best fit.
[d] Best fit using $c_1=3.5\times10^{-4}$ mol/g.
[e] Best fit using p$\bar{K}$=6.74.
[f] Best fit using p$\bar{K}$=6.74 and $c_1=5.3\times10^{-4}$ mol/g.
[g] Best fit using p$\bar{K}$=6.74 and $c_1=3.5\times10^{-4}$ mol/g.
[h] Best fit using p$\bar{K}$=9.08 and $c_1=3.5\times10^{-4}$ mol/g.

three isotherms described reasonably well the experimental data, but the difference between the predicted and experimental adsorption isotherms remained larger than the precision of our experimental data. The modeling analysis of the three adsorption isotherms together only poorly constrained the $p\bar{K}$ value of the reactive site, as the sites of type 1 were excluded but not the sites of type 2 or of type 3. On the other hand, the $p\bar{T}'$ value could be estimated as equal to about -1.2 ± 0.1. If the electrostatic effects are neglected, ψ_0=0, the $p\bar{K}$ and $p\bar{T}'$ values are equal to the pK and pT' values of the reactive sites. Instead, if we consider ψ_0=-0.38, the pK values are equal to $p\bar{K}-0.38$, and the pT' values are equal to $p\bar{T}'-0.38$. For instance, a $p\bar{T}'$ value of -1.22 can be interpreted as a pT' value of -1.60, while a $p\bar{K}$ value of 6.74 is equivalent to a pK value of 6.36.

It is interesting to compare our results with those obtained for the adsorption of other divalent cations onto *B. subtilis* cells. For instance, Fein et al. (1997), who took into account the electrostatic effects through a constant capacitance model, reported a pT' value of -1.42 ± 0.25 for the adsorption of cadmium onto the dominant reactive sites, which they proposed to be the carboxylic sites (pK=4.82). However, they could not obtain a good fit with only carboxylic sites, and they had to introduce sites with a higher pK value (pK=6.90). They proposed that the sites with the higher pK value were contributing to the adsorption at the higher pH values. Using their data and our modeling protocol, we were however able to obtain an excellent fit by considering only one site. For instance, considering the adsorption isotherm of $10^{-4.05}$ M of cadmium onto about 850 dry mg of bacteria (Fein et al., 1997), the best fits we could obtain has a precision on the order of 1.94 μM. For instance, using a $p\bar{K}$ value equal to 6.90, the best fit was obtained for a site concentration of 1.05×10^{-4} mol/g and $p\bar{T}'=-0.47$, which led to Δ=1.95 μM. Fits with a precision smaller than 3 μM could only be obtained for $p\bar{K}$ values larger than 5.95. Imposing a site concentration of 3.6×10^{-4} mol/g, as suggested by Kulczycki et al. (2002), the best fit was obtained for a $p\bar{K}$ value of 6.17 and a $p\bar{T}'$ value of -1.19 and had a precision of 2.84 μM. For a site concentration of 3.5×10^{-4} mol/g and a $p\bar{K}$ value of 6.74, the best fit was obtained for a $p\bar{T}'$ value of -1.20 and had a precision of 3.18 μM. These values are strikingly close to those that we obtained for the modeling of the adsorption isotherms of the ferrous ions using similar constraints (Tables 2 and 3). They suggest that ferrous and cadmium divalent cations adsorb quite identically onto bacterial surfaces. Many other divalent cations are adsorbing more easily, such as lead or copper, and some with more difficulty, such as calcium or strontium (Fein et al., 1997, 2001; Kulczycki et al., 2002; Ngwenya et al., 2003).

3.3.3. Modeling of the adsorption data: two-site model

We modeled each adsorption isotherm using a two-site model. This refinement of the model did not allow us to obtain any improvement of the fit for the adsorption isotherm at 5 g/l or for the three adsorption isotherms modeled together. However, this does not prove that only one type of sites

Table 4
Parameters characterizing various fits obtained by searching for the highest possible affinity for the sites of type 1 (two-site model)

Bacterial concentration of the selected isotherm (dry weight)	Precision of the fit Δ (10^{-6} M)	Concentrations of the two types of reactive sites (10^{-4} mol/dry g of bacteria)		$p\bar{K}$ values of the two types of reactive sites		Adsorption constants of the two types of reactive sites			
						$p\bar{T}$		$p\bar{T}'$	
		c_1	c_2	$p\bar{K}_1$	$p\bar{K}_2$	$p\bar{T}_1$	$p\bar{T}_2$	$p\bar{T}'_1$	$p\bar{T}'_2$
50 mg/l	1.93	5.60	5.30	4.45	6.74	3.92	−0.53	4.11	−2.63
	1.99	2.00	5.30	4.45	6.74	4.79	0.34	4.36	−2.38
500 mg/l	1.98	5.60	2.70	4.45	6.74	3.35	−1.10	5.48	−1.26
	1.99	2.00	2.50	4.45	6.74	3.80	−0.65	5.58	−1.16
5 g/l	5.99	5.60	5.30	4.45	6.74	2.56	−1.89	5.13	−1.61
	5.98	2.00	5.30	4.45	6.74	3.01	−1.44	5.13	−1.61
All three isotherms	5.97	5.60	4.50	4.45	6.74	2.96	−1.49	5.20	−1.54
	5.98	2.00	4.50	4.45	6.74	3.40	−1.05	5.21	−1.53

contributed significantly to the adsorption of the ferrous ions. Our results, as described and discussed in Section 3.3.2, suggest that the contribution of the sites of type 1, with a $p\bar{K}$ of 4.45, was not dominant. We used the two-site model to investigate further this question and evaluate the maximal potential contribution of the sites of type 1, as allowed by the experimental data. For this, we considered that the bacterial surfaces were covered with the sites of type 1, as suggested by the titration ($p\bar{K}_1$=4.45, c_1= 5.6×10^{-4} mol/g), and with the sites of type 2 ($p\bar{K}_2$=6.74), with a concentration equal to at most 5.3×10^{-4} mol/g. Using these constraints, we could obtain optimal fits for the adsorption isotherms at 50 and 500 mg/l as long as the adsorption constant of the ferrous ions onto the type 1 sites was kept lower than or equal to $p\bar{T}'$ =−0.53 (50 mg/l) or −1.10 (500 mg/l). The corresponding fits are shown in Table 4. For the adsorption isotherm at 5 g/l, fits with a precision lower than 6 μM could be obtained for $p\bar{T}'_1$ larger than −1.89 (see Table 4). Modeling all three adsorption isotherms together, fits with a precision lower than 6 μM could be obtained for larger than −1.49 (see Table 4).

We also considered the possibility that some of the sites of type 1 might not have been available to the ferrous ions and assumed that their concentration was equal to $c_1=2\times10^{-4}$ mol/g instead of $c_1=5.6\times10^{-4}$ mol/g. Using these constraints, we could obtain optimal fits for the adsorption isotherms at 50 and 500 mg/l as long as the adsorption constant of the ferrous ions onto the type 1 sites was kept lower than or equal to $p\bar{T}'_1$ =0.34 (50 mg/l) or −0.65 (500 mg/l). The corresponding fits are shown in Table 4. For the adsorption isotherm at 5 g/l, fits with a precision lower than 6 μM could be obtained for $p\bar{T}'$ larger than -1.44 (see Table 4). Modeling all three adsorption isotherms together, fits with a precision lower than 6 μM could be obtained for $p\bar{T}'_1$ larger than −1.05 (see Table 4).

Using Eq. (11), the fraction of ferrous ions adsorbed onto the sites of type 1 and onto the sites of type 2 could be calculated for any given fit. This is shown on Fig. 6, for the case where $c_1=5.4\times10^{-4}$ mol/g. The case where $c_1=2\times10^{-4}$ mol/g was quite similar, and it is thus not shown here. Considering only the adsorption isotherm at 50 mg/l, it was possible to obtain a fit according to which the type

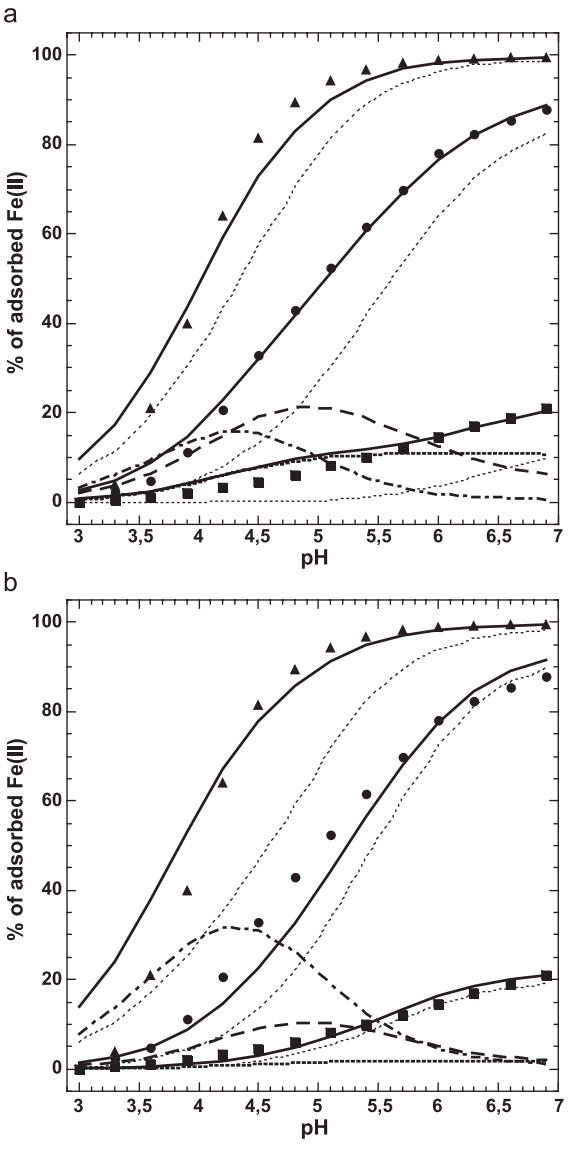

Fig. 6. Adsorption isotherms: experimental data for the adsorption isotherm at 48 mg/l (■), 456 mg/l (●), and 5.3 g/l (▲); prediction of the two-site models using the parameters of Table 4 with $c_1=5.6\times10^{-4}$ mol/g for the three isotherms examined individually (a) or together (b). Percentage of Fe(II) adsorbed on the sites of type 2 as thin dotted lines; percentage of Fe(II) adsorbed on the sites of type 1 as bold dotted line (48 mg/l), bold dashed line (456 mg/l), and bold dotted–dashed line (5.3 g/l). Note that the sum of the contributions of the sites of type 1 and of the sites of type 2 is equal to the prediction of the two-site model, which is shown as full bold lines.

1 sites were dominant at low and intermediate pH conditions. However, for the adsorption isotherm at 500 mg/l, the contribution of the type 1 sites was dominant only at low pH values, up to about pH 4.5–5.0 at the most. For the adsorption isotherm at 5 g/l, no dominant contribution of the sites of type 1 could be introduced, even at low pH. Modeling all three adsorption isotherms together, it was also found that no significant contribution of the sites of type 1 could be introduced above pH 4.0–4.5, even for the adsorption isotherm at 50 mg/l (Fig. 6b). It is important to keep in mind that Fig. 6 represents the maximal potential contribution of the sites of type 1 in the two-site model, and that their actual contribution might be much smaller. Altogether, the modeling of the adsorption isotherms with a two-site model indicated that the sites of type 1 were not needed to describe the experimental data and that they might have contributed only to a minor fraction of the adsorption except, possibly, in the low pH range (pH<4.5). It also indicated that an adsorption isotherm at a single bacterial concentration is insufficient to make conclusions regarding the nature of the reactive sites.

4. Conclusion

In this paper, we have demonstrated that ferrous ions do adsorb reversibly onto the surface of *B. subtilis*, and that the adsorption equilibrium is reached within minutes. The adsorption isotherms are similar to those obtained in previous studies for other metallic divalent cations and in particular to those obtained with cadmium ions. The concentration of detected reactive sites was on the order of 16 and 3.5×10^{-4} mol per dry g of bacteria for the protons and for the ferrous ions, respectively. The titration data revealed the presence of at least three types of proton-reactive sites, with $p\bar{K}$ values of 4.45, 6.74, and 9.08, respectively. Several previous studies have obtained similar titration curves, but the relationship between the proton-reactive sites detected by the titrations and those detected by biochemical analyses of the cells enveloppes is still unresolved. Our adsorption data and modeling analysis indicated that only one kind of sites was needed to predict adsorption isotherms of ferrous ions onto *B. subtilis* cells. The sites with a $p\bar{K}$ value of 4.45 likely played a small role in the adsorption process, even at low pH conditions. The sites with a $p\bar{K}$ of 6.74 were the best candidates as dominant reactive sites for adsorption. In most previous studies, it has been proposed that the sites with a low p*K* (p*K*=4.45 in our case) were carboxylic sites and that they were often the dominant sites for the adsorption of metallic cations. We have shown that such conclusions may have to be reconsidered in some instances. Studies examining the adsorption of metallic cations onto bacterial cells using biochemical or spectroscopic techniques have suggested that either phosphodiester or carboxylic groups are the dominant reactive groups, depending on the pH or on the nature of the cation considered (Beveridge and Murray, 1980; Boyanov et al., 2003; Hennig et al., 2001; Kelly et al., 2001; Panak et al., 2000, 2002a,b; Sarret et al., 1998). These sites are believed to have p*K* values lower or equal to 5. Hence, there is an apparent contradiction between the experimental data obtained by titration and batch adsorption experiments, and the data obtained using other techniques. Because the realization of adsorption isotherms is the best way to obtain quantitative information on the values of the adsorption constants of the reactive sites, we believe that identifying the chemical nature of the reactive sites, as detected by the titration/adsorption data, is a critical point, which still needs to be resolved. We have also shown that determining a "best fit" for a single adsorption isotherm is a somewhat meaningless task, as many different sets of parameters can fit the data almost equivalently well. Rather, acceptable families of fits should be determined. Fitting a set of adsorption isotherms realized at different bacteria/metal ratios can also restrict efficiently the number of parameters leading to a good fit of the data. We have proposed here that all of our data can be best and most simply fitted when either the sites of type 2 or the sites of type 3 are the dominant reactive sites, with a concentration of 3.5×10^{-4} mol/g and an adsorption constant $p\tilde{T}'$ equal to about -1.2. However, our best fits were still insufficiently good with respect to the quality of the experimental data. In particular, we were unable to properly describe the adsorption isotherm at 5g/l, even by taking into account two kinds of sites or by trying to use various available

electrostatic models (not shown here). The development of better models, which will take into account the complex and three dimensional structure of the bacterial enveloppes may be needed to achieve a good description of the adsorption isotherms and to resolve the apparent discrepancies between the data obtained by spectroscopic and biochemical techniques and those obtained by batch adsorption experiments.

Meanwhile, our results are already of importance with respect to the study of the cycle of iron and associated elements at redox boundaries. They indicate for instance that bacterial cell surfaces can significantly reduce the dissolved concentration of Fe(II), thereby reducing the kinetics of the oxidation/hydrolysis reaction in the bulk of the precipitation reaction of a Fe(III) solid phase. However, the adsorption is reversible and the exchange between the adsorbed and desorbed Fe(II) should not be neglected in a system where the chemical conditions vary over time. In an oxic system, this exchange should ultimately lead to the oxidation of most of the Fe(II) either as an adsorbed species on the cells surface or, at least, in the bulk phase. Various questions still need to be investigated quantitatively. For instance, the kinetic of oxidation of the adsorbed Fe(II) in oxygenated conditions have not yet been measured, as well as the potential role of adsorbed Fe(II) on the activity of iron-reducing bacteria in anoxic conditions.

Acknowledgments

We thank Paul Kenward for helping in the laboratory and Chris Daughney for useful discussions and for fitting our experimental data with FITEQL 2.0® and with various electrostatic models. This project was partially funded by an NSERC grant to D. Fortin. **[LW]**

References

Achouak, W., Thomas, F., Heulin, T., 1994. Physico-chemical surface properties of rhizobacteria and their adhesion to rice roots. Colloids Surf., B Biointerfaces 3, 131–137.

Archibald, A.R., 1989. The *Bacillus* cell enveloppe. In: Harwood, C.R. (Ed.), Bacillus. Plenum Press, pp. 217–254.

Beveridge, T.J., Murray, R.G.E., 1980. Sites of metal deposition in the cell wall of *Bacillus subtilis*. J. Bacteriol. 141 (2), 876–887.

Boyanov, M.I., Kelly, S.D., Kemner, K.M., Bunker, B.A., Fein, J.B., Fowle, D.A., 2003. Adsorption of cadmium to *Bacillus subtilis* bacterial cell walls: a pH-dependent X-ray absorption fine structure spectroscopy study. Geochim. Cosmochim. Acta 67 (18), 3299–3311.

Châtellier, X., Fortin, D., West, M.M., Leppard, G.G., Ferris, F.G., 2001. Effect of the presence of bacterial surfaces during the synthesis of Fe oxides by oxidation of ferrous ions. Eur. J. Mineral. 13, 705–714.

Châtellier, X., West, M.M., Rose, J., Fortin, D., Leppard, G.G., Ferris, F.G., 2004. Characterization of iron-oxides formed by oxidation of ferrous ions in the presence of various bacterial species and inorganic ligands. Geomicrobiol. J. 21 (3), 99–112.

Cornell, R.M., Schwertmann, U., 2003. The Iron Oxides. Wiley-VCH.

Daughney, C.J., Fein, J.B., 1998. The effect of ionic strength on the adsorption of H^+, Cd^{2+}, Pb^{2+}, and Cu^{2+} by *Bacillus subtilis* and *Bacillus licheniformis*: a surface complexation model. J. Colloid Interface Sci. 198, 53–77.

Daughney, C.J., Fowle, D.A., Fortin, D., 2001. The effect of growth phase on proton and metal adsorption by *Bacillus subtilis*. Geochim. Cosmochim. Acta 65 (7), 1025–1035.

Emerson, D., 2000. Microbial oxidation of Fe(II) and Mn(II) at circumneutral pH. In: Lovley, D.R. (Ed.), Environmental Microbe–Metal Interactions. ASM Press, pp. 31–52.

Fein, J.B., Daughney, C.J., Yee, N., Davis, T.A., 1997. A chemical equilibrium model for metal adsorption onto bacterial surfaces. Geochim. Cosmochim. Acta 61 (16), 3319–3328.

Fein, J.B., Martin, A.M., Wightman, P.G., 2001. Metal adsorption onto bacterial surfaces: development of a predictive approach. Geochim. Cosmochim. Acta 65 (23), 4267–4273.

Ferris, F.G., Beveridge, T.J., Fyfe, W.S., 1986. Iron–silica crystallite nucleation by bacteria in a geothermal sediment. Nature 320, 609–611.

Fortin, D., Ferris, F.G., 1998. Precipitation of iron, silica, and sulfate on bacterial cell surfaces. Geomicrobiol. J. 15, 309–324.

Fortin, D., Ferris, F.G., Beveridge, T.J., 1997. Surface-mediated mineral development by bacteria. In: Banfield, J.F., Nealson, K.H. (Eds.), Geomicrobiology: Interactions Between Microbes and Minerals, vol. 35. Mineralogical Society of America, pp. 161–180.

Fortin, D., Ferris, F.G., Scott, S.D., 1998. Formation of Fe-silicates and Fe-oxides on bacterial surfaces in samples collected near hydrothermal vents on the Southern Explorer Ridge in the northeast Pacific Ocean. Am. Mineral. 83, 1399–1408.

Francis, C.A., Tebo, B.M., 2002. Enzymatic manganese(II) oxidation by metabolically dormant spores of diverse *Bacillus* species. Appl. Environ. Microbiol. 68 (2), 874–880.

Hennig, C., Panak, P.J., Reich, T., Rossberg, A., Raff, J., Selenska-Pobell, S., Matz, W., Bucher, J.J., Bernhard, G., Nitsche, H., 2001. EXAFS investigation of uranium (VI) complexes formed at *Bacillus cereus* and *Bacillus sphaericus* surfaces. Radiochim. Acta 89, 625–631.

Kelly, S.D., Boyanov, M.I., Bunker, B.A., Fein, J.B., Fowle, D.A., Yee, N., Kemner, K.M., 2001. XAFS determination of the

bacterial cell wall functional groups responsible for complexation of Cd and U as a function of pH. J. Synchrotron. Radiat. 8, 946–948.

Kelly, S.D., Kemner, K.M., Fein, J.B., Fowle, D.A., Boyanov, M.I., Bunker, B.A., Yee, N., 2002. X-ray absorption fine structure determination of pH-dependent U-bacterial cell wall interactions. Geochim. Cosmochim. Acta 66 (22), 3855–3871.

Kennedy, C.B., Martinez, R.E., Scott, S.D., Ferris, F.G., 2003. Surface chemistry and reactivity of bacteriogenic iron oxides from axial Volcano, Juan de Fuca Ridge, north-east Pacific Ocean. Geobiology 1, 59–69.

Kulczycki, E., Ferris, F.G., Fortin, D., 2002. Impact of cell wall structure on the behavior of bacterial cells as sorbents of cadmium and lead. Geomicrobiol. J. 19, 553–565.

Langmuir, D.A., 1997. Aqueous Environmental Chemistry. Prentice Hall.

Liu, C., Zachara, J.M., Gorby, Y.A., Szecsody, J.E., Brown, C.F., 2001. Microbial reduction of Fe(III) and sorption/precipitation of Fe(II) on shewanella putrefaciens strain CN32. Environ. Sci. Technol. 35 (7), 1385–1393.

Lovley, D.R., 2000. Fe(III) and Mn(IV) reduction. In: Lovley, D.R. (Ed.), Environmental Microbe–Metal Interactions. ASM Press, pp. 3–30.

Madigan, M.T., Martinko, J.M., Parker, J., 2003. Brock Biology of Microorganisms. Prentice Hall.

Marsh, D., 1990. Handbook of Lipid Bilayers. CRC Press.

Martinez, R.E., Ferris, F.G., 2001. Chemical equilibrium modeling techniques for the analysis of high-resolution bacterial metal sorption data. J. Colloid Interface Sci. 243, 73–80.

Martinez, R.E., Smith, D.S., Kulczycki, E., Ferris, F.G., 2002. Determination of intrisic bacterial surface acidity constants using a donnan shell model and a continuous pK_a distribution method. J. Colloid Interface Sci. 253, 130–139.

Mozes, N., Handley, P.S., Busscher, H.J., Rouxhet, P.G., 1991. Microbial Cell Surface Analysis. VCH Publishers.

Ngwenya, B.T., Sutherland, I.W., Kennedy, L., 2003. Comparison of the acid–base behaviour and metal adsorption characteristics of a Gram-negative bacterium with other strains. Appl. Geochem. 18, 527–538.

Okuda, S., Igarashi, R., Kusui, Y., Kasahara, Y., Morisaki, H., 2003. Electrophoretic mobility of *Bacillus subtilis* knockout mutants with and without flagella. J. Bacteriol. 185 (13), 3711–3717.

Opekarova, M., Tanner, W., 2003. Specific requirements of membrane proteins—a putative bottleneck in heterologous expression. Biochim. Biophys. Acta 1610, 11–22.

Panak, P.J., Booth, C.H., Caulder, D.L., Bucher, J.J., Shuh, D.K., Nitsche, H., 2002. X-ray absorption fine structure spectroscopy of plutonium complexes with *Bacillus sphaericus*. Radiochim. Acta 90, 315–321.

Panak, P.J., Knopp, R., Booth, C.H., Nitsche, H., 2002. Spectroscopic studies on the interaction of U(VI) with *Bacillus sphaericus*. Radiochim. Acta 90, 779–783.

Panak, P.J., Raff, J., Selenska-Pobell, S., Geipel, G., Bernhard, G., Nitsche, H., 2000. Complex formation of U(VI) with *Bacillus*-isolates from a uranium mining waste pile. Radiochim. Acta 88, 71–76.

Roden, E.E., Urrutia, M.M., 2002. Influence of biogenic Fe(II) on bacterial crystalline Fe(III) oxide reduction. Geomicrobiol. J. 19, 209–251.

Sarret, G., Manceau, A., Spadini, L., Roux, J.-C., Hazemann, J.-L., Soldo, Y., Eybert-Bérard, L., Menthonnex, J.-J., 1998. Structural determination of Zn and Pb binding sites in *Penicillium chrysogenum* cell walls by EXAFS spectroscopy. Environ. Sci. Technol. 32, 1648–1655.

Schultze-Lam, S., Fortin, D., Davis, B.S., Beveridge, T.J., 1996. Mineralization of bacterial surfaces. Chem. Geol. 132, 171–181.

Shelobolina, E.S., Vanpraagh, C.G., Lovley, D.R., 2003. Use of ferric and ferrous iron containing minerals for respiration by desulfitobacterium frappieri. Geomicrobiol. J. 20 (2), 143–156.

Southam, G., 2000. Bacterial surface-mediated mineral formation. In: Lovley, D.R. (Ed.), Environmental Microbe–Metal Interactions. ASM Press, pp. 257–276.

Stryer, L., 1996. Biochemistry. W. H. Freeman and Company.

Stumm, W., Morgan, J.J., 1996. Aquatic Chemistry. John Wiley and Sons.

Urrutia, M.M., Roden, E.E., 1998. Microbial and surface chemistry controls on reduction of synthetic Fe(III) oxide minerals by the dissimilatory iron-reducing bacterium *Shewanella alga*. Geomicrobiol. J. 15, 269–291.

Viollier, E., Inglett, P.W., Hunter, K., Roychoudhury, A.N., Van Cappellen, P., 2000. The ferrozine method revisited: Fe(II)/Fe(III) determination in natural waters. Appl. Geochem. 15, 785–790.

Westall J. C., 1982. FITEQL: A Computer Program for Determination of Chemical Equilibrium Constants from Experimental Data; version 2.0, pp. 101. Department of Chemistry, University of Oregon.

Westall, J., Hohl, H., 1980. A comparison of electrostatic models for the oxide/solution interface. Adv. Colloid Interface Sci. 12, 265–294.

Wolfram, S., 1997. Mathematica. International Thomson Publishing.

Yee, N., Fein, J.B., 2001. Cd adsorption onto bacterial surfaces: a universal adsorption edge? Geochim. Cosmochim. Acta 65 (13), 2037–2042.

Yee, N., Phoenix, V.R., Konhauser, K.O., Benning, L.G., Ferris, F.G., 2003. The effect of cyanobacteria on silica precipitation at neutral pH: implications for bacterial silicification in geothermal hot springs. Chem. Geol. 199 (1–2), 83–90.